Computational Fluid Dynamics Simulation Of Multiphase System Of Gas-Liquid Flow In A Vertical Pipeline

Liz Wong Sze Ming
School of Engineering
Asia Pacific University of Technology and Innovation (APU)
Kuala Lumpur, Malaysia
tp055718@mail.apu.edu.my

Muhammad Syahmi Afif Bin Mokhtar Yazid
School of Engineering
Asia Pacific University of Technology and Innovation (APU)
Kuala Lumpur, Malaysia
syahmi.afif@apu.edu.my

Juhairi Aris Bin Muhamad Shuhili
Department of Business and Management,
Universiti Teknologi Mara Perak Branch Tapah Campus,
Perak Darul Ridzuan, Malaysia
juhairiaris@gmail.com

Rosli Yusop
School of Engineering
Asia Pacific University of Technology and Innovation (APU)
Kuala Lumpur, Malaysia
rosli.yusop@apu.edu.my

Adeline Sneha John Chrisastum
School of Computing
Asia Pacific University of Technology and Innovation (APU)
Kuala Lumpur, Malaysia
adeline.john@apu.edu.my

Muhammad Adidinizar Bin Zia Ahmad Kusairee
Department of Business and Management,
Universiti Teknologi Mara Perak Branch Tapah Campus,
Perak Darul Ridzuan, Malaysia
adidi627@uitm.edu.my

***Abstract* — This study presents a computational fluid dynamics (CFD) simulation of a multiphase system of gas-liquid flow in a vertical pipeline. The main aim of this research is to evaluate the effect of flow pattern on the influence of holdup, void fraction, and liquid film thickness for concurrent flow of air and liquid in a vertical pipe. The proposed method employs ANSYS Fluent to work on the multiphase simulation. The study shows that the accuracy of the results increases with an increase in the number of times steps and decreases in the time step size. The results of the simulation were compared with published results, and they were found to be less than 10% of errors. The findings of this study can be useful in understanding the behaviors of gas-liquid flows in vertical pipelines and can be applied in various engineering fields, such as chemical and petroleum industries.**

Keywords— Computational Fluid Dynamics (CFD), Menter's Shear Stress Transport (SST), Renormalization Group (RNG), Reynolds Stress Model (RSM), Wax Appearance Temperature (WAT)

I. INTRODUCTION

Studies were conducted for 2-D and 3-D simulation for two-phase flow in vertical pipe using CFD commercial software revealed that the nature of the flow vary in accordance with the cross-sectional configuration. 3D simulation showed a more superior result than 2D (Abdulkadir, Hernandez-Perez, Lo, Lowndes, & Azzopardi, 2015). Pressure drops played a significant role, primarily attributed to the frictional effects between fluids and the internal walls of pipes and piping systems (Yang, 2020). As the investigation focused on vertical pipes, pressure drop became a crucial parameter. The alteration of flow patterns within the pipes held vital implications for pressure drop, particularly with regards to the safety of pipeline transportation (Adaze, Badr, & Al-Sarkhi, 2019). Numerous studies have addressed pressure drop phenomena in vertical pipe systems. An observation was made that an increase in bubble flow leads to a corresponding pressure drop in vertical pipes. The air flow increased as the pressure dropped. Understanding the relationship between flow patterns and pressure drop was essential in assessing pipeline safety and optimizing flow assurance measures (Chen, Tian, & Karayiannis, 2006; Cheng, Hills, & Azzorpardi, 1998).

The determination of liquid holdup held significant importance in the design of multiphase flow pipes and closely linked to the pressure gradient within the pipe. This relationship served as a fundamental basis for the design and analysis of oil and gas wells (Li, Wang, Yousaf, Yang, & Ishii, 2018) . Accurate calculation of liquid holdup facilitated the prediction of gas quantities present in the pipeline. An observation made revealed that an increase in liquid holdup is directly proportional to the pipe diameter for a given gas-liquid ratio. Understanding and accurately determining the liquid holdup aided in optimizing pipeline design and predicting the behavior of multiphase flow systems (Ganat & Hrairi, 2018).

Void fraction in gas-liquid flow referred to the proportion of a channel's volume occupied by the gas phase, or the percentage of the channel's cross-sectional area occupied by the gas phase. Throughout this study, particular attention was given to the behavior of void fraction in vertical pipes, as that exhibited distinct characteristics across different scenarios (Xu, et al., 2022).Increasing in the gas superficial velocity led to an increase in the void fraction. This increase in void fraction was accompanied by a corresponding decrease in pressure values. Understanding the dynamics of void fraction is essential for comprehending the intricate nature of gas-liquid flow in vertical pipes and its impact on system performance (Gardenghi, et al., 2020).

CFD mesh refers to the process of generating a numerical grid in computational fluid dynamics simulations. Similar to meshing in finite element simulations, CFD meshing involves applying a grid to both the fluid body and its boundaries. The accuracy and precision of a CFD simulation heavily depend on the grid points created through meshing methods (Ren, et al., 2021). To evaluate the reliability of

simulation results, a mesh independence study is often conducted. This study involves running multiple simulations using different mesh resolutions and examining whether the outcomes remain consistent. By doing so, it becomes possible to determine if the simulation results are independent of the underlying mesh used in the analysis (Gayet, Diaye, & Line, 2013; Liang, Guo, & Wang, 2021)

A 3D generalization of a 2D quadrilateral mesh is a hexahedral mesh which does not always have a cubic or cartesian arrangement of points. Meshes made of distorted cubes are produced via hexahedral or hexahedra meshing (Wang, Zheng, & Xu, 2019). Such meshes can considerably increase both speed and accuracy, which is why they are frequently used to simulate specific types of physics such as deformation mechanics and fluid dynamics (Wongwises & Pipathattakul, 2006). Using hex dominant meshing in pipelines consists of 3 main stages, which are compute a global parameterization, then generate hexahedra and extract the remaining void. Lastly, re-mesh the void (Gray & Ormiston, 2021; Liu, Sun, Lu, Song, & Yu, 2015).

A tetrahedral mesh serves as a three-dimensional extension of a two-dimensional triangular mesh. In the context of computational modeling, tetrahedral elements are commonly employed to discretize three-dimensional domains. These elements can take the form of isosceles tetrahedra when asymmetries are present, while equilateral tetrahedra are utilized in systems exhibiting circular curvature (Shawkat, Ching, & Shoukri, 2008). Tetrahedral meshes offer the advantage of being highly flexible and adaptable to complex geometries, allowing for accurate representation of arbitrary shapes. Compared to simpler cubic grids in 3D or square grids in 2D, tetrahedral meshes provide significantly enhanced accuracy in numerical simulations (Hibiki & Mishima, 2001; Lote, Vinod, & Patwardhan, 2018).

The Cartesian cut cell methodology provides an appealing alternative to traditional body-fitted or unstructured meshing methods. For complex geometries, it enables quick, automatic mesh production while maintaining the computational benefits of using Cartesian grids. An appropriate surface mesh must be provided as an input for cartesian meshing to work. There are some requirements on that surface mesh that, if they are not met, may either result in a subpar final mesh or may result in the Cartesian meshing process failing (Kiran, Ahmed, & Salehi, 2020; Mahmood, 2019). The boundary layer resulting from the no-slip condition at the buoy is captured using a prism layer mesh surrounding the floating module The total number of layers, growth rate, and first layer thickness are all specified for the prism layer mesh. This kind of layer has the benefit of effectively resolving boundary layer (Mishima & Ishii, 1984; Yadav, Kim, Tien, & S. M. Bajorek, 2014).

Turbulence modeling refers to the development and utilization of mathematical models to predict the behavior of turbulence. In the field of computational fluid dynamics (CFD), turbulent models are employed to forecast the evolution of turbulence in various real-world turbulent flows (Sim, Bae, & Mureithi, 2010). These models utilize simplified constitutive equations that capture the statistical characteristics of turbulent flows. Computational fluid dynamics encompasses a wide range of turbulence schemes, each employing different approaches to simulate and analyze turbulent phenomena (Li, Zhang, & Lu, 2019; Razzaghi, Amjad, & Maleki, 2020).

II. METHODS

Ansys Fluent computer simulation had 3 stages of process. There was pre-processing stage, processing stage and the post processing stage. Started at the pre-processing stage, the design of the simulation was defined. In the processing stage, there was the pipe's geometry modelling and the pipe's mesh sizing. To find the best mesh sizing for this simulation, mesh independence study was needed. Then, the mesh was setup by choosing a type of mesh either hex dominant, tetrahedron, cartesian or prism. For this case, it was probably tetrahedron. The skewness must be less than 90%. If it's less than 90%, it will proceed to the turbulence scheme, where there are k-epsilon and k-omega. When mesh independence study and turbulence scheme are done, it will proceed to the Fluent simulation setup. It is setup either using toolbox or coding.

After that, the boundary condition and the model equations were determined. Mesh setup or mesh independence study or turbulence scheme process were repeated to have the correct boundary conditions and model equations. The simulation was started after all the previous process had no errors. Then, the residual convergence must be less than 0.0001. If not, the previous process needed to be repeated to check the errors. If the residual convergence is less than 0.0001 then the results will be recorded as the end. The post-processing process involved the checking of residual convergence until the end of the results. procedure for creating the software model in Ansys Fluent was depicted in the flowchart in the Figure 1.

Pre-processing, processing, and post-processing were the three processes that make up the simulation process. As seen, each stage is connected to the others. For instance, the proper mesh selection and boundary condition setting might lead to convergence of a better outcome. In the pre-processing step, in addition to the various mesh types that could be used for the model, such as tetra and quads, the definition of the design, meshing, modelling geometry, and simulation setup take place. The mesh size and mesh study were chosen independently to produce accurate findings. In general setup, we need to determine the boundary conditions and governing equations. The simulation is for gas-liquid flow so there will be the superficial velocity of air and the superficial velocity of water. The configuration of the system was shown in Figure 3 and Figure 4.

The inlet boundary for two-phase flow:

Superficial velocity of air: $Ua = \frac{Qa}{Am}$

Superficial velocity of water: $Uw = \frac{Qw}{Am}$

Where Am=Aa+Aw

The outlet boundary for two phase flow:

$$\frac{dUm}{dx} = \frac{dVm}{dy} = \frac{dWm}{dz} = 0$$

The mixture of two-phase flow is assumed to be no-slip boundary condition on the wall of the pipe: $Um = Vm = Wm = 0$.

According to the volume fraction values for each phase, the balance of mass and momentum equations in the governing equations of flow provide an explanation for the solution of (air-water) two-phase flow through a domain. The general of continuity equation, Equation 1 for mixture of flow:

$$\frac{d\rho m}{dt} + \frac{d}{dxi}(\rho Um) = 0$$

Equation 1: Continuity Equation

The general of momentum equation, Equation 2 for mixture flow:

$$\frac{d(\rho mUj)}{dt} + \frac{d}{dxj}(\rho mUiUj) = -\frac{dp}{dxi} + \rho mgj + \frac{d}{dxj}\left[\mu m\left(\frac{dUj}{dxj} + \frac{dUj}{dxi}\right) - \rho m\overline{u'\imath u'_j}\right] + \bar{F}$$

Equation 2: Momentum Equation

There is a parameter to be calculated before the simulation, assume r=2cm, R=2.5cm & r=2cm, R=1cm.

$$\frac{r}{R}, \frac{2}{2.5} = 0.8 \;\&\; \frac{2}{1} = 2$$

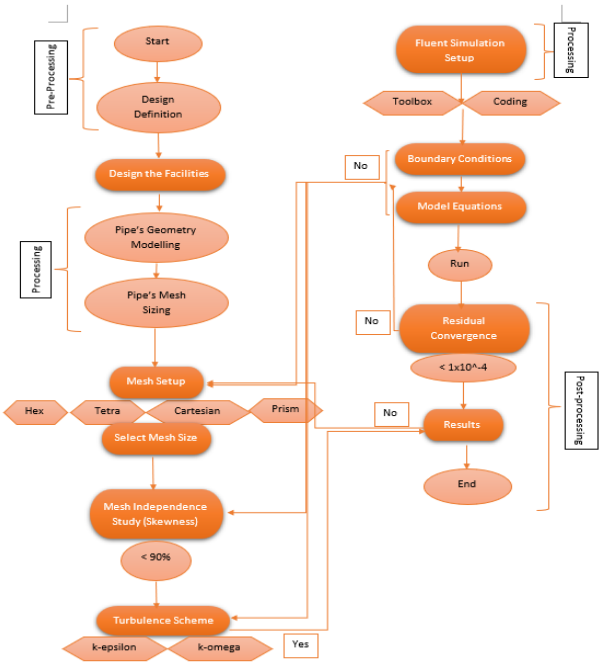

Figure 1: Methodology Process Flow Chart

The experimental campaign began by describing the test fluids for the research, as shown in the table below. Waxy Terengganu crude oil from Malaysia and filtered water were used as test fluids throughout the entire testing process. The waxy crude oil used for the research was categorized as mild waxy crude oil because of its low WAT and low pour point of 25°C and 18°C, respectively. Filtered water was chosen to be fed into the facility to ensure that only liquid-liquid flow took place in the system.

The system implementation of ANSYS Fluent involves several key steps. Firstly, the appropriate geometry for the simulation is created using Design Modeler. Design Modeler is a 3D CAD software that is included with ANSYS Fluent. The geometry created was then updated then the appropriate mesh is created using the meshing tools. The mesh should be fine enough to accurately capture the flow behavior, but not too fine as to be computationally expensive. The appropriate physical models and boundary conditions were then specified, and the simulation was run. It was important to perform a convergence analysis to ensure that the results are accurate and have reached a steady state. Finally, the results can be analyzed and visualized using post-processing tools, ANSYS CFD-Post.

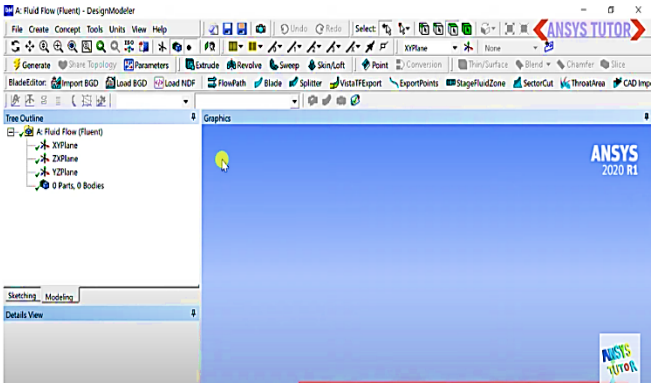

Figure 2: Design Modeler Interface

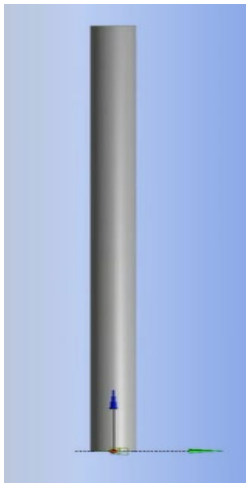

Figure 3: Vertical Pipe Geometry

The experimental set-up was designed as an inlet air-water flow is co-current through the 2m vertical pipe. The behavior of flow patterns (bubble, slug, churn) was obtained by using VOF homogenous model with unsteady turbulent mixture flow. The evolution of the two-phase flow was studied in a vertical pipe with a diameter of 50mm as shown in Figure 5 supplied with air and water. The inlet mixture flow (air and water) was co-current to get matching between the air and water superficial velocities. It was assumed that air was the first phase, and the water was the second phase with giving the value of surface tension 0.0704 at 35° c. Assume the volume fraction of water to the body 1, this

means the body will be filled with water and then air enters to get more accurate distribution patterns.

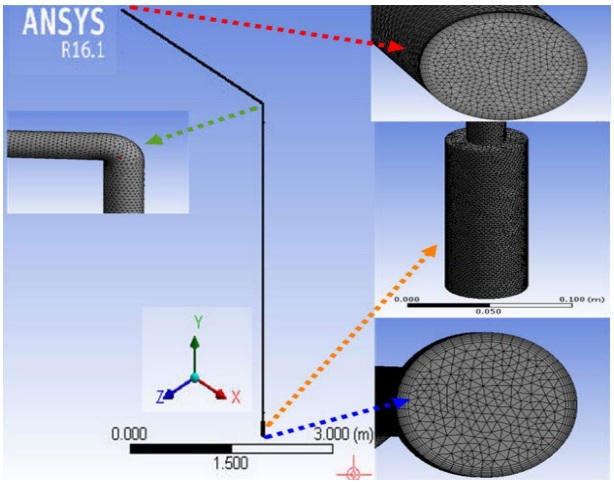

Figure 4: Unstructured Mesh for Vertical Pipe

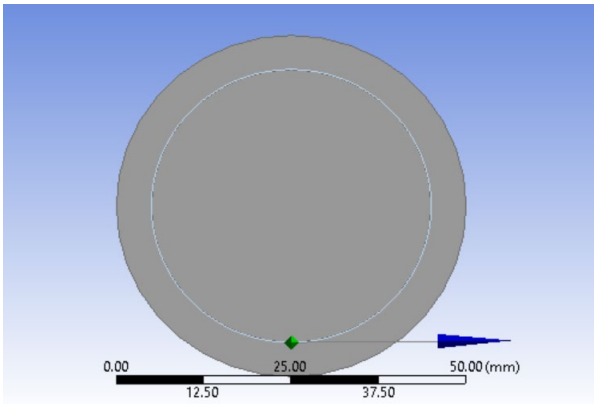

Figure 5: Pipe Diameter

The simulation covered the general setup in ANSYS Fluent to test the gas-liquid flow includes geometry design, mesh generation, setup, solution, and results.

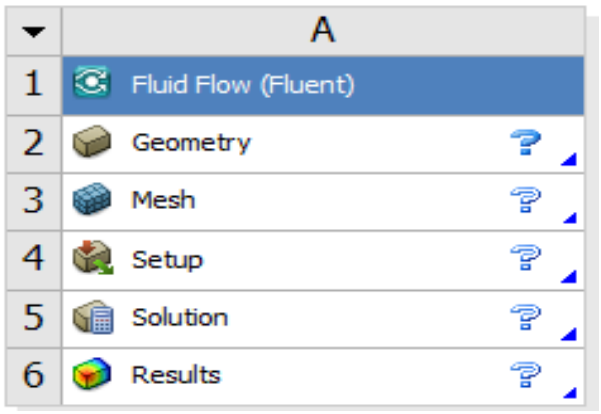

Figure 6: Ansys Fluent Setup

The simulation set-up was explained below:

1. Define the geometry of the vertical pipe: Using Solidworks , create a 3D model of the vertical pipe that accurately represents the dimensions.
2. Set up the CFD simulation: Define the fluid properties, such as density, viscosity, and surface tension, as well as the boundary conditions, such as flow rate, pressure, and temperature and the material properties.
3. Run the simulation: The CFD software will then use numerical methods to solve the equations governing the flow, providing information about the velocity, pressure, and temperature fields within the vertical pipe.
4. Analyze the results: Interpret and analyze the results of the simulation to understand the behavior of the gas-liquid flow in the vertical pipe.
5. Validate the results: Compare the simulation results to experimental data to validate the accuracy of the model.

The design of the vertical pipe was done by using Design Modeler in ANSYS Fluent. Due to limitations in computational resources, a vertical pipe with a length of 2 meters and a diameter of 0.05 meters was chosen for simulation. This length was selected as the laptop used for the simulation was not able to handle the computational demands of a longer pipe length, such as 100 meters or more. While this length may not be representative of all real-world applications, it provides a reasonable approximation for evaluating the effect of flow pattern based on the influence of holdup, void fraction, and liquid film thickness for concurrent flow of air and liquid in a vertical pipe. The results of this study can still provide valuable insights into the behavior of gas-liquid flows in vertical pipelines and can be used as a foundation for further research on longer pipe lengths. The pipe geometry is shown in the Figure 7.

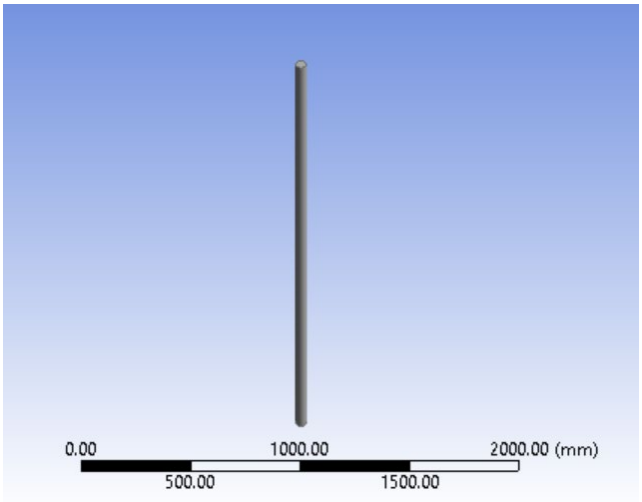

Figure 7: Pipe Geometry in Design Modeler

In the simulation, a multiphase flow consisting of air and water is considered. Therefore, the inlet was projected onto two separate surfaces, one for the air phase and one for the water phase as shown in Table 1. This was necessary because the two phases had different properties and behavior, and therefore require separate treatment in the simulation. By projecting the inlet onto separate surfaces, the flow properties for each phase can be specified independently, such as velocity and volume fraction. This allows for a more accurate simulation of the multiphase flow in the pipeline.

Table 1: Phases in the Pipe Inlet

Inlet of Air	Inlet of Water
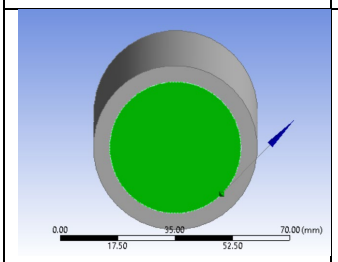	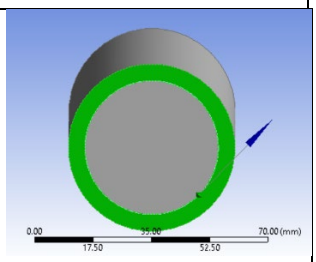

Once the geometry of the pipe was complete, the next step was to generate the mesh for the simulation. The first step in mesh generation was to define the sizing for the elements. In this case, an element size of 0.005 meters was selected as it provides a good balance between accuracy and computational efficiency for the given case. Next, the meshing method was defined using multizone, which divided the geometry into separate regions or zones for more efficient meshing. This method was particularly useful for complex geometries with varying properties, such as those found in multiphase flow simulations.

After the multizone method was selected, the next step was to add inflation to the wall of the pipe. Inflation involved adding additional mesh layers near the wall to capture the boundary layer effects, which are critical for accurately modelling fluid flows near a solid surface. In this case, five layers of inflation were added to the wall of the pipe to ensure accurate modelling of the frictional effects of the liquid-water with the pipe wall. After completing the mesh generation process, the resulting mesh for the simulation consists of 114,600 nodes and 107,587 elements as shown in Figure 8.

Details of "Mesh"

Solver Preference	Fluent
Element Order	Linear
Element Size	5.e-003 m
Export Format	Standard
Export Preview Surface Mesh	No
Sizing	
Quality	
Inflation	
Batch Connections	
Advanced	
Statistics	
Nodes	114600
Elements	107587

Figure 8: Element Size & Statistics

The quality of the mesh can be evaluated using metrics such as skewness, which measures the deviation of the shape of a mesh element from an ideal shape. In this case, the mesh metric data shows that the maximum skewness is less than 0.9, which is within an acceptable range for most simulations and the average skewness is around 0.15, which indicates an excellent cell quality for the mesh as shown in Figure 9. A lower average skewness indicates that the mesh elements are closer to an ideal shape, which can improve the accuracy and stability of the simulation results.

Mesh Metric	Skewness
Min	1.3445e-002
Max	0.83291
Average	0.15619
Standard Deviation	0.15171

Figure 9: Mesh Metric Details

Once the mesh is generated, the next step is assigning boundary conditions to named surfaces, which are identified using named selection. In this case, four surfaces were identified for the simulation: inlet air, inlet water, wall, and outlet. Each of these surfaces corresponds to a specific region of the geometry and requires a different boundary condition to be applied. For simulating multiphase flows of water and air, the pressure-based and transient model is used. In this model, the governing equations of fluid flow are solved in a pressure-based framework, where the pressure and velocity fields are coupled through the continuity equation. This allows for more accurate representation of the fluid behavior at the free surface and around the pipe geometry. For fluid flows with gravity, such as the case of water and air interactions, the gravity term is included in the governing equations to account for the effect of buoyancy. Hence, a value of -9.81 m/s² is used to represent the acceleration due to gravity.

The simulation will be using the VOF model to study the behaviour of a two-phase flow system consisting of air and water. The VOF model is a popular method used to simulate two-phase flows, and it tracks the volume fractions of the two phases throughout the domain. For phases section, air will be the primary phase and water will be the secondary phase. As for the surface tension coefficient, 0.0704 was used. Regarding the surface tension force modelling, wall adhesion was selected. The wall adhesion model assumes that the liquid phase wets the wall completely, which is a reasonable assumption for most practical cases, such as bubble or droplet formation. Additionally, the wall adhesion method is computationally efficient and requires fewer parameters compared to the jump adhesion method, which can simplify the setup and reduce the computational cost of the simulation. For the turbulence scheme, different turbulence model is tested to evaluate the effect of the flow regime. Two commonly used turbulence models are the k-epsilon and k-omega models. The tested models are k-epsilon standard, k-epsilon RNG, k-epsilon Realizable, k-omega standard and k-omega SST. To choose the most suitable turbulence model for a given flow, the characteristics of the flow need to be analysed.

Once the turbulence model has been chosen, the next step in setting up a two-phase flow simulation is to define the boundary conditions for each phase, specifically their velocities. For the air phase, the boundary conditions will depend on the specific characteristics of the flow, such as the velocity and direction of the air stream. Typically, the inlet velocity of the air phase will be specified at the inlet boundary, while the outlet boundary will be set to a zero gradient condition to allow the air to exit the domain freely.

For the water phase, the boundary conditions will also depend on the specific characteristics of the flow, such as the velocity and direction of the water stream. In general, the inlet velocity of the water phase will be specified at the inlet boundary, while the outlet boundary will be set to a pressure outlet condition to allow the water to exit the domain freely. Two different cases are tested, and the results are recorded as shown in Table 2.

Table 2: Air Velocity & Water Velocity for Case1 & Case 2

	Case 1	Case 2
Air Velocity	0.11m/s	0.2m/s
Water Velocity	1.3m/s	14m/s

The outlet boundary condition defines the behavior of the fluid as it exits the simulation domain. In this case, the gauge pressure at the outlet is specified as 1 atm, which is equivalent to 101325 Pa. This means that the fluid pressure at the outlet will be maintained at this value throughout the simulation, ensuring that the flow exits the domain smoothly and without any backflow. There are several different pressure-velocity coupling schemes that can be used, one common pressure-velocity coupling scheme is the SIMPLE (Semi-Implicit Method for Pressure-Linked Equations) algorithm, which is an iterative method that solves for both the pressure and velocity fields simultaneously. Another widely used coupling scheme is the PISO (Pressure-Implicit with Splitting of Operators) algorithm, which also solves for the pressure and velocity fields iteratively but uses a splitting of the Navier-Stokes equations to improve the stability and convergence of the solution. Hence, SIMPLE and PISO are selected, and their results are recorded.

Before starting the simulation, it is important to initialize the data by setting the initial conditions for the fluid properties, including the water volume fraction. In this case, the water volume fraction is set to 1, which means that the entire simulation domain is filled with water at the beginning of the simulation. Lastly, the number of time steps and time step size would need to be specified before running the simulation. The number of time steps will depend on the duration of the simulation and the desired time resolution. More time steps and smaller time step size generally lead to more accurate results, as they allow the simulation to capture more of the dynamics and fluctuations of the flow. This is because smaller time steps allow for more precise calculation of the time derivatives in the governing equations, which can improve the accuracy of the numerical solution. However, using too many time steps and small-time size can significantly increase the computational cost and time required to run the simulation.

III. RESULT AND DISCUSSION

Once the simulation results were generated, they were loaded into CFD-post for visualization and analysis. CFD-post was a post-processing tool that is used to visualize and analyze simulation results generated by a CFD solver. The simulation results provided insights into the system's performance and served as a basis for future research and development activities. A mesh independence study was a process in which the effect of different mesh sizes on the accuracy of a computational fluid dynamics (CFD) simulation was evaluated. The objective was to determine the appropriate mesh size that provides accurate results while also being computationally efficient.

Mesh size referred to the size of the elements or cells that made up the meshed geometry of the vertical pipe. A smaller mesh size implied a higher resolution of the model, allowing for more accurate representation of the geometry, and capturing finer details and features of the multiphase flow being simulated. However, a smaller mesh size also meant that the number of elements or cells increased, leading to a longer simulation time. Meanwhile, there was a limitation to the numbers of elements and cells in the student license of ANSYS Fluent.

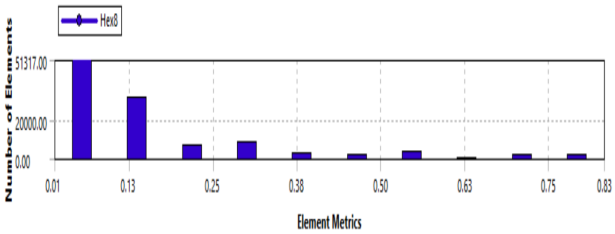

Figure 10: Number of Elements vs Element Metrics

As shown in Figure 10, elements metrics that were more than 0.13 would not be sufficient. Therefore, by considering the computational budget, the mesh size of 0.005mm was chosen. The mesh size of 0.005mm was enough for the simulation model to has a suitable level of detail, with 107587 elements with 114600 nodes. This could be appropriate for simulating vertical pipe geometries, and it was enough to capture accurate fine features and small variations. In general, it ws recommended to use the smallest possible mesh size that meets the accuracy requirements, while considering the computational cost and simulation time. The contour volume was shown in Figure 11 and Figure 12.

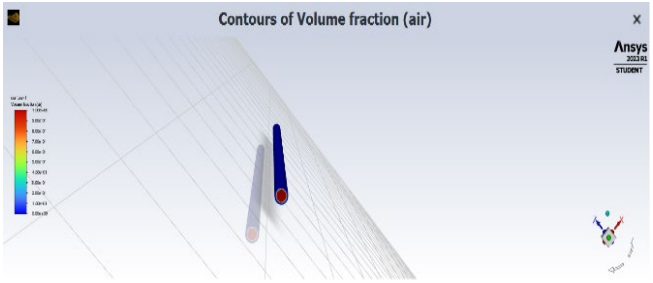

Figure 11: Contours of Volume Fraction of Air before the simulation

The vertical pipe had an inlet located below it and an outlet located above it. The inlet would have a mixture of water and gas. During the setup, the water had volume fraction of 1 which meant that only water was initially present in the pipe. After running the simulation, one scenario was that the water would flow downward due to gravity, while the gas would flow upward due to buoyancy. This could create a stratified flow pattern with the water at the bottom and the gas at the top of the pipe. As the mixture flew upward, the gas bubbles might expand due to the decreasing pressure, which

can lead to a decrease in the water volume fraction and the formation of gas pockets. Other flow patterns were slug flow or annular flow, depending on the flow rates.

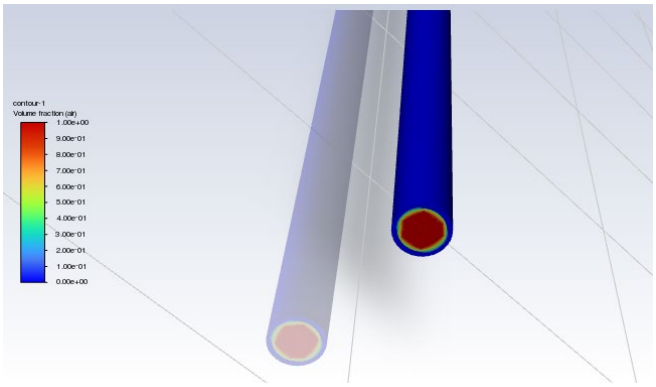

Figure 12: Zoom In of Contour of Volume Fraction of Air before the simulation

Scope	
Scoping Method	Geometry Selection
Geometry	1 Body
Definition	
Suppressed	No
Boundary Scoping Method	Geometry Selection
Boundary	1 Face
Inflation Option	Smooth Transition
Transition Ratio	Default (0.272)
Maximum Layers	5
Growth Rate	1.2
Inflation Algorithm	Pre

Figure 13: Inflation Details

Inflation involved creating a boundary layer of cells that were smaller and denser near the solid surface to capture the fluid flow gradients and velocity profiles in this region as shown in Figure 13. Smooth transition inflation method was chosen, it was a method that smoothly increased the cell size from the interior of the domain to the surface of the solid boundary. This was achieved by gradually increasing the cell size ratio from the interior to the boundary, rather than using a sudden jump in cell size at the boundary. The cell size ratio was the ratio of the size of the first layer of cells adjacent to the boundary to the desired size of the cells in the interior of the domain.

The data utilized in this study were provided in Table 3.

Table 3: Details of Phases

Phase	Type	Density (kg/m³)	Viscosity (kg/(ms))
Air	Primary	1.225	1.7894e-05
Water	Secondary	998.2	0.001003

The default transition ratio for smooth transition inflation in ANSYS Fluent is 0.272, which meant that the cell size ratio was increased by a factor of 0.272 at each layer. The maximum number of layers was set to 5, which meant that there would be a maximum of 5 layers of cells adjacent to the solid boundary. In Fluent, a common practice was to use a five-layer mesh inflation, which means that the mesh was gradually inflated over five layers of cells starting from the solid surface. A five-layer mesh inflation was used in the simulations because it provided a good balance between accuracy, efficiency, and consistency.

Flow pattern for Ua=0.11m/s, Uw=1.3m/s was slug flow as shown in Figure 14.

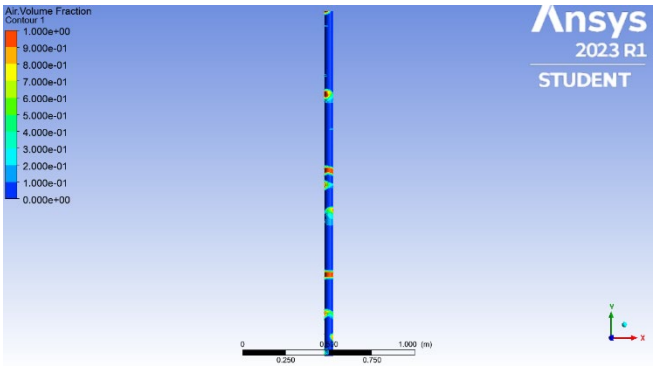

Figure 14: Slug Flow Pattern

Slug flow was characterized by the periodic formation of large gas pockets (slugs) separated by liquid plugs. In this case, the air and water flow rates were such that large gas pockets (slugs) were expected to form periodically in the pipe, separated by liquid plugs. This type of flow pattern was typically observed at low gas flow rates and high liquid flow rates, based on the given conditions.

Flow pattern for Ua=14m/s, Uw=0.2m/s was annular flow as shown in Figure 15.

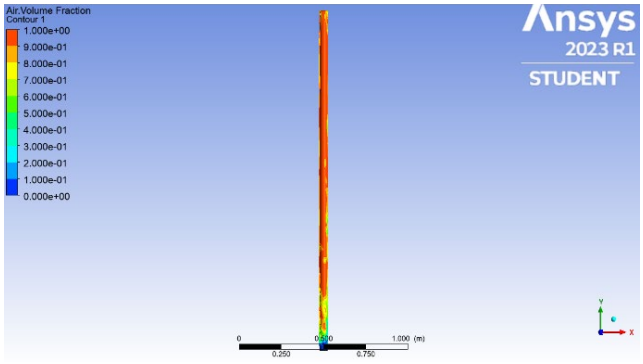

Figure 15: Annular Flow Pattern

The annular flow was characterized by the air which predominantly flows through the central core of the pipe, where a liquid film surrounded the inner wall of the pipe. In annular flow, the gas phase flows at a higher velocity compared to the liquid phase, resulting in a thin film of liquid adhering to the pipe wall. The liquid film was typically continuous, while the gas flew as a dispersed phase through the center of the pipe. The flow pattern had presence of a distinct interface between the liquid film and the gas core.

Therefore, it was concluded that the transition between flow patterns depended on the air superficial velocity and water superficial velocity. The proposed design for computational fluid dynamics (CFD) of air-water flew in a vertical pipe aims to achieve three objectives. Firstly, to propose the optimum number of mesh based on the

unstructured shape and size for a mesh independence study. Secondly, to evaluate the effect of the flow regime based on the selection of turbulence scheme. Thirdly, to compare the influence of liquid hold-up, void fraction, and liquid film thickness on pressure drop through the vertical pipes.

The proposed design would involve conducting a series of simulations using Fluent software, varying the number of mesh elements and turbulence schemes while keeping the geometry and flow conditions constant. The results would then be analyzed to determine the optimal mesh size and turbulence model for the simulation, and to identify the key parameters that affect the pressure drop in vertical pipes. 10 CFD simulation are tested with varying air velocity, water velocity, turbulence model, pressure-velocity coupling scheme, numbers of time step and time step size (s) as shown as table below:

Table 4: Simulation's Details

Simulation	Air Velocity & Water Velocity	Turbulence Model	Pressure-Velocity Coupling Scheme	Numbers of Time Step	Time Step Size (s)
A	Ua=0.11m/s Uw=1.3m/s	k-epsilon (Standard)	PISO	300	0.01
B	Ua=14m/s Uw=0.2m/s	k-epsilon (Standard)	PISO	300	0.01
C	Ua=0.11m/s Uw=1.3m/s	k-epsilon (RNG)	PISO	300	0.01
D	Ua=0.11m/s Uw=1.3m/s	k-epsilon (Realizable)	PISO	300	0.01
E	Ua=0.11m/s Uw=1.3m/s	k-omega (SST)	PISO	300	0.01
F	Ua=0.11m/s Uw=1.3m/s	k-omega (Standard)	PISO	300	0.01
G	Ua=0.11m/s Uw=1.3m/s	k-epsilon (Realizable)	SIMPLE	300	0.01
H	Ua=14m/s Uw=0.2m/s	k-epsilon (RNG)	SIMPLE	300	0.01
I	Ua=0.11m/s Uw=1.3m/s	k-epsilon (Realizable)	PISO	3000	0.001
J	Ua=14m/s Uw=0.2m/s	k-epsilon (RNG)	PISO	3000	0.001

In addition to the three objectives outlined previously, the proposed design for computational fluid dynamics (CFD) of air-water flow in a vertical pipe includes validation of the simulation results through comparison with experimental data. Each test would be explained in detail, including the experimental setup, data collection, and analysis of the test data. By comparing the simulation and experimental results, the accuracy and reliability of the simulation can be assessed, and any discrepancies can be identified and analyzed. This validation process will provide confidence in the accuracy of the simulation results and demonstrate the usefulness of the proposed design for practical applications in industry. The findings of this study will be useful in designing and optimizing vertical pipe systems for various industrial applications.

In the case of a 2m long and 0.05m diameter pipe, different meshing methods such as tetrahedrons, hex dominant, sweep, multizone, and cartesian can be used to create the mesh. Each method had its advantages and disadvantages as shown in Table 5.

Defaults	
Physics Preference	CFD
Solver Preference	Fluent
Element Order	Linear
Element Size	5.e-002 m
Export Format	Standard
Export Preview Surface Mesh	No

Table 5:Element Size used 0.05m

When using Ansys Student License, the number of mesh elements that could be used for a simulation was limited. This limitation was typically in terms of the maximum number of elements or nodes that could be included in the simulation. Therefore, it was essential to be cautious when defining the element size in the mesh because, if the element size was too small, it would result in many elements that would exceed the maximum grid cells allowed by the Ansys Student License. The element size of the cells in a mesh was a critical parameter in a CFD simulation. Smaller elements could improve the accuracy of the simulation by capturing the local flow features, such as turbulence eddies and boundary layer separation. However, it came at the cost of increased computational resources, such as processing power, memory, and storage. When using Ansys Student License, the maximum number of elements was typically limited, and it was necessary to optimize the mesh to get the best possible results within this limit. This meant that the element size should be chosen carefully to ensure that the simulation was both accurate and efficient. The chosen element size was 0.005m with 5 layers of inflation as shown in Table 6.

Method	Mesh Geometry	Mesh Metric & Statistics
Automatic & Tetrahedron	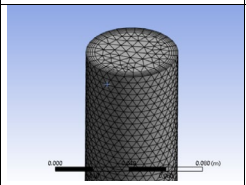	Details of "Mesh" Target Skewness: Default (0.9) Smoothing: Medium Mesh Metric: Skewness Min: 5.0936e-004 Max: 0.79985 Average: 0.19498 Standard Deviation: 0.13741 Inflation Batch Connections Advanced Statistics Nodes: 103659 Elements: 267081
Hex Dominant	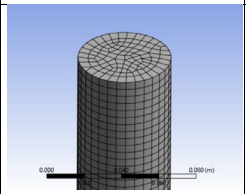	Details of "Mesh" Target Skewness: Default (0.9) Smoothing: Medium Mesh Metric: Skewness Min: 2.5891e-002 Max: 1. Average: 0.40183 Standard Deviation: 0.2848 Inflation Batch Connections Advanced Statistics Nodes: 63304 Elements: 69372
Multizone	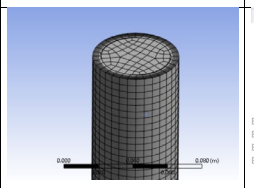	Details of "Mesh" Target Skewness: Default (0.9) Smoothing: Medium Mesh Metric: Skewness Min: 1.3445e-002 Max: 0.83291 Average: 0.15619 Standard Deviation: 0.15171 Inflation Batch Connections Advanced Statistics Nodes: 114600 Elements: 107587
Cartesian	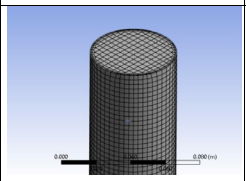	Details of "Mesh" Target Skewness: Default (0.9) Smoothing: Medium Mesh Metric: Skewness Min: 1.3057e-010 Max: 0.50968 Average: 0.12958 Standard Deviation: 0.12259 Inflation Batch Connections Advanced Statistics Nodes: 183074 Elements: 167682

Table 6: Mesh Details

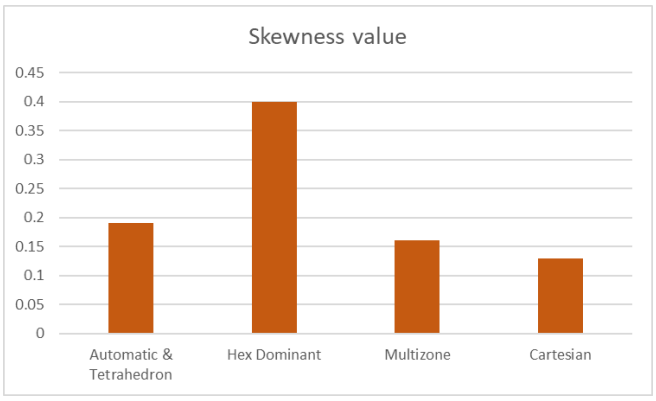

Figure 16: Different Method's Skewness Value

The hex dominant had no inflation layer because hexahedral elements did not have curved faces. The inflation layer required a layer of elements with curved faces, a smooth transition from the bulk flow to the boundary layer, which could be challenging and difficult to achieve with hexahedral elements. The least value of skewness was cartesian method but in the case of a vertical pipe, the geometry was cylindrical, and the use of a Cartesian mesh would result in a highly distorted mesh near the curved walls. The skewness was shown in Figure 16. This would lead to inaccuracies in the simulation results, as the mesh elements near the walls would not accurately capture the fluid flow behavior. Instead, the second least skewness value which was multizone meshing was chosen. The multizone method can generate high-quality meshes that were more structured and had a better distribution of elements than other techniques. This could lead to faster convergence rates and better numerical stability.

For simulating air-water flow in a pipe, a pressure-based solver is used. Pressure-based solver, the governing equations are discretized using the pressure-velocity coupling method. The pressure-velocity coupling method solves the pressure and velocity equations separately, which allows the use of larger time steps and can lead to faster convergence compared to density-based solvers. In the case of simulating air-water flow in a vertical pipe, a transient simulation is typically more appropriate because it allows capturing the dynamic behavior of the bubbles as they move through the pipe. A steady-state simulation assumes that the flow properties remain constant with time, and it is useful for problems where the flow is steady and does not change with time. However, in the case of air-water flow, the flow properties change with time as the air move through the pipe, so a steady-state simulation may not capture the full behavior of the system. Therefore, for simulating air-water in a vertical pipe, it was a transient simulation in ANSYS Fluent.

Turbulence Model		Results
k-omega	SST	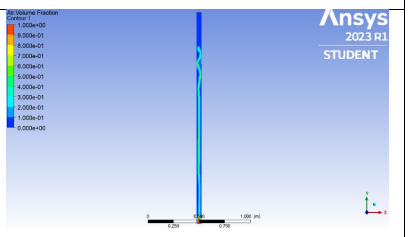
	Standard	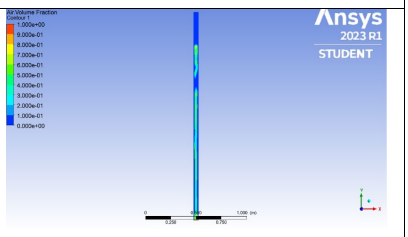
k-epsilon	Standard	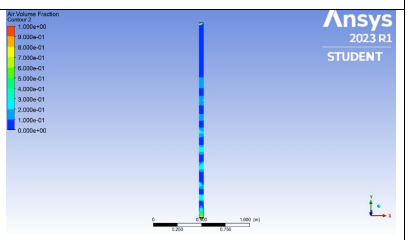
	RNG	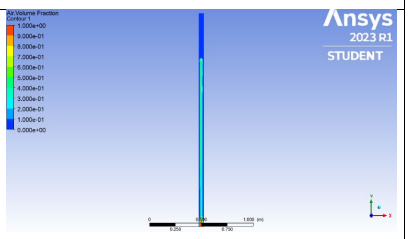

Figure 17: Flow Pattern of Simulations

For the air water velocity and water velocity there were Case 1 and Case 2. The use of Case 1 and Case 2 velocities suggested that there are 2 different flow conditions. These tests are tested based using either Case 1 or Case 2 velocity with different method either k-epsilon and k-omega with either PISO or SIMPLE. The simulation of A-H is using time step of 300 and time step size of 0.01 to test the flow pattern while simulation of I & J were using time step of 3000 and

time step size of 0.001. Since the time step size in the simulation of I & J was smaller, it could be expected to have a higher accuracy than the simulation of A-H. However, this also means that the simulation of I & J had taken longer to compute than the simulation of A-H due to the smaller time step size. Therefore, the flow pattern for Case 1 velocity is shown in simulation I and the flow pattern for Case 2 velocity is shown in simulation J.

In this research, the k-epsilon and k-omega turbulence models were selected to compare their performance in predicting the air-water flow behavior in a vertical pipe. First, a 2m vertical pipe with a diameter of 0.05m in the ANSYS Design Modeler was created as shown in Figure 18. Then, generate a mesh to discretize the geometry into small control volumes using multizone method. After that, define the fluid properties, such as the density and viscosity of the liquid and gas phases. Following by specifying the boundary conditions for the simulation. For the inlet, set the volumetric flow rates of the liquid and gas phases. For the outlet, set the pressure or velocity boundary condition. Hereafter, select a suitable turbulence model, such as the k-epsilon or k-omega. Then, initialized the solution and run the simulation. In the Post-processing stage, analyzed the flow pattern in the simulation using air volume fraction.

Turbulence Model		Results
k-omega	SST	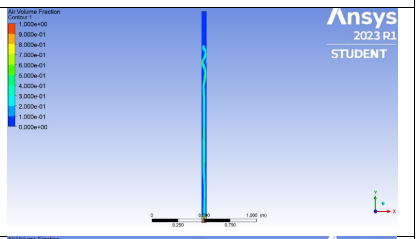
	Standard	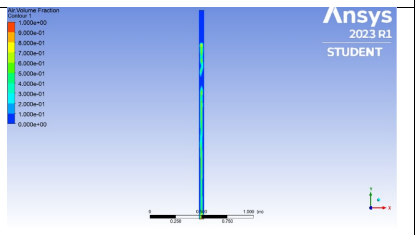
k-epsilon	Standard	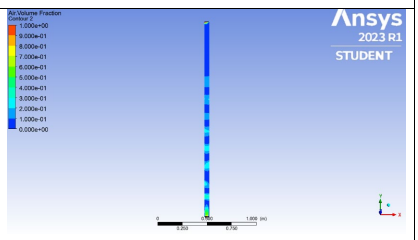
	RNG	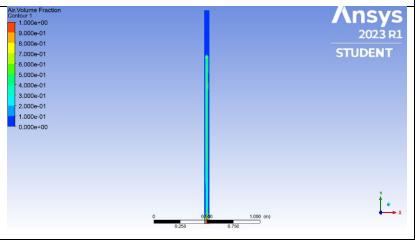

Figure 18: Flow Pattern of Different Turbulence Method

Then, the solver settings were configured, including the selection of the turbulence model (e.g., k-epsilon, k-omega) that best represents the flow characteristics. The numerical discretization schemes for solving the governing equations were chosen to ensure accuracy and stability. Convergence criteria were defined to determine when the solution had reached a satisfactory level of convergence. The time step size was determined based on stability and accuracy considerations, considering the dynamic behavior of the flow. Boundary conditions play a crucial role in defining the behavior of the flow at the inlet, outlet, and pipe walls. The inlet conditions specified the air and water velocities, phase fractions. The outlet conditions were typically set to atmospheric pressure (101325pa). The pipe walls were defined as no-slip walls, assuming zero velocity at the wall boundary. Before starting the simulation, the initial conditions of the flow variables were specified throughout the computational domain. These initial conditions provided a starting point for the simulation and were often based on physical understanding or estimated values.

Once the transient simulation is completed, post-processing was carried out to analyze and visualize the results of flow pattern. The simulation results could be compared with experimental data to validate the accuracy of the simulation and gain insights into the flow characteristics as shown in Figure 17.

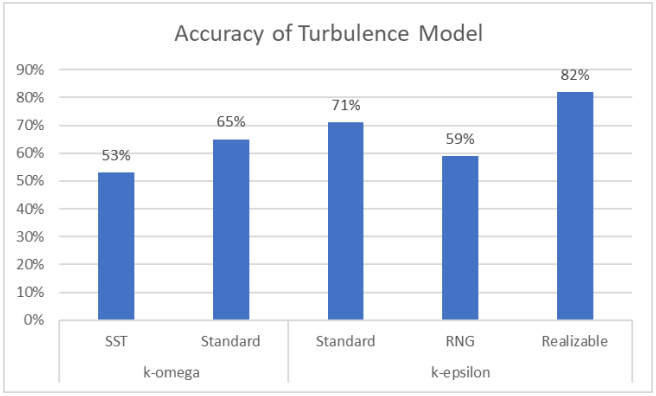

Figure 19: Accuracy of Turbulence Model

In the context of a multiphase flow of air and water in a vertical pipe, different turbulence models were used to predict the flow behavior, and each model exhibited varying levels of accuracy. The k-omega (SST) turbulence model achieved an accuracy of 53% in predicting the flow pattern. This model considered the turbulent kinetic energy (k) and specific dissipation rate (omega) to capture the turbulence characteristics. However, the relatively lower accuracy suggests that it might have struggled to accurately capture the complex multiphase interactions and flow phenomena occurring in the vertical pipe.

On the other hand, the k-epsilon turbulence model performed slightly better, with the standard variant achieving a flow pattern accuracy of 71%. This model divided the turbulent kinetic energy (k) and dissipation rate (epsilon) to model the turbulent flow. It was known for its versatility and robustness in various engineering applications, and in this case, it provided relatively more accurate predictions of the flow pattern compared to the k-omega (SST) model.

The RNG (Reynolds Number-specific) variant of the k-epsilon turbulence model achieved an accuracy of 59%. The RNG model introduced additional modifications to the standard k-epsilon model based on the Reynolds number,

aiming to improve its predictive capabilities. However, in this specific multiphase flow scenario, it exhibited a lower accuracy compared to the standard k-epsilon model. The Realizable turbulence model demonstrated the highest accuracy among the models, with an accuracy of 82% in predicting the flow pattern. The Realizable model considered the Reynolds stress and aims to capture the complex interactions between turbulence components more accurately. Its improved accuracy suggests that it was better suited for capturing the intricate multiphase flow phenomena occurring in the vertical pipe.

Based on the accuracy results provided, the k-epsilon turbulence model emerged as the most suitable scheme for simulating air-water flow in a vertical pipe. A 2m vertical pipe with a diameter of 0.05m in the ANSYS Design Modeler was created. A mesh was generated to discretize the geometry into small control volumes using multizone method. After that, the fluid properties were defined, such as the density and viscosity of the liquid and gas phases. The boundary conditions for the simulation were specified. For the inlet, volumetric flow rates of the liquid and gas phases were set. For the outlet, the pressure or velocity boundary condition was set. Hereafter, a suitable turbulence model, such as the k-epsilon or k-omega was selected. Then, the solution was initialized, and the simulation was run. In the post-processing stage, the results of liquid holdup were analyzed in the simulation.

Table 7: Pressure Drop of Simulation

Simulation	Pressure (Pa)		Pressure Difference
	Min	Max	
A	101318	101330	12
B	101325	103331	2006
C	101325	119203	17878
D	101294	101326	32
E	101325	119186	17861
F	101325	119886	18561
G	101312	101343	31
H	101254	101370	116
I	101319	101334	15
J	101323	103264	1941

The pressure differences observed in the simulations as shown in Table 7 could be attributed to various factors, including the air and water velocities, turbulence models, pressure-velocity coupling schemes, and the number and size of time steps as shown in Figure 11. In Simulation A, with an air velocity of 0.11 m/s and a water velocity of 1.3 m/s, the pressure difference was relatively small at 12 Pa. This suggested a relatively steady and well-balanced flow condition. In Simulation B, where the air velocity was significantly higher at 14 m/s and the water velocity was lower at 0.2 m/s, the pressure difference increased to 2006 Pa. This indicated a larger pressure drop along the pipeline due to the higher air velocity causing increased turbulence and flow disturbances.

Comparing to Simulation A and Simulation C, where the same air and water velocities were used but different turbulence models were employed, it is observed that the pressure difference remained the same at 12 Pa. This suggested that the choice of turbulence model did not significantly impact the pressure distribution in this scenario. Similarly, comparing Simulation A and Simulation D, where different turbulence models k-epsilon Realizable vs. k-epsilon Standard were used, the pressure difference remained relatively small at 32 Pa. This further supported the finding that the turbulence model had a limited influence on the pressure distribution in this specific flow configuration.

In Simulation E and Simulation F, where the k-omega turbulence model was used instead of the k-epsilon model, the pressure differences were 17861 Pa and 18561 Pa, respectively. These larger pressure differences indicated higher pressure drops along the pipeline compared to the cases with the k-epsilon turbulence model. In Simulation G, where the pressure-velocity coupling scheme was changed from PISO to SIMPLE while using the k-epsilon Realizable turbulence model, the pressure difference remained similar at 31 Pa. This suggested that the choice of coupling scheme had a limited effect on the pressure distribution in this case.

Comparing Simulation H, Simulation J, and Simulation B, where the same turbulence model (k-epsilon RNG) was used but different air and water velocities were applied, it was observed that the pressure differences increased as the air velocity decreased, and the water velocity increased. This indicated that higher air velocities and lower water velocities resulted in larger pressure drops along the pipeline. Finally, by comparing Simulation I and J with Simulation A and B, it was proven that reducing the time step size (from 0.01 s to 0.001 s) while maintaining the same simulation parameters did not significantly impact the pressure difference.

Hence, the pressure differences observed in the simulations were influenced by the velocities of air and water, turbulence models, pressure-velocity coupling schemes, and the flow conditions. Higher air velocities, lower water velocities, and certain turbulence models (such as k-omega) tended to result in larger pressure drops along the pipeline, indicating more significant flow disturbances and turbulence.

Table 8: Simulations of Liquid Holdup

Simulation	Volume (mm)		Liquid Holdup
	Liquid Volume	Pipe Volume	
A	62832	78540	0.798727
B	1571	78540	0.019493
C	54978	78540	0.698727
D	58905	78540	0.74618
E	51051	78540	0.651273
F	53407	78540	0.682544
G	58120	78540	0.741278
H	785	78540	0.00974
I	68323	78540	0.873733
J	6283	78540	0.078724

A 2m vertical pipe with a diameter of 0.05m in the ANSYS Design Modeler was created. A mesh was generated to discretize the geometry into small control volumes using multizone method. After that, the fluid properties were defined, such as the density and viscosity of the liquid and gas phases. The boundary conditions for the simulation were

specified. For the inlet, volumetric flow rates of the liquid and gas phases were set. For the outlet, pressure or velocity boundary condition were set. Hereafter, a suitable turbulence model was selected, such as the k-epsilon or k-omega. Then, solution was initialized, and simulation was run. In the post-processing stage, the results of liquid holdup were analyzed in the simulation.

Liquid holdup formula:

$$Hl = \frac{Vl}{V}$$

Equation 3: Liquid Hold Up Formula

Hl=liquid holdup

Vl=pipeline segment volume occupied by liquid

V=whole pipeline segment volume

For a 2m pipe with 0.05m diameter vertical pipe, the volume is 78540mm³.

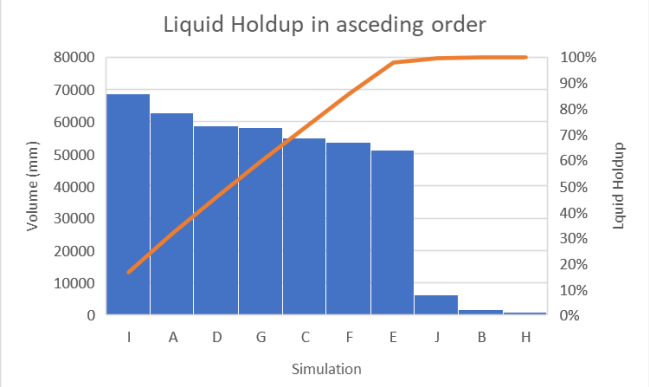

Figure 20: Liquid Holdup of Simulations in order

The computation of liquid hold-up was done using Equation 3 and the results were shown in Table 8 and Figure 20. Simulations A, C, D, E, F, G, and I had the same air velocity (Ua = 0.11 m/s) and water velocity (Uw = 1.3 m/s), while Simulations B, H, and J had different velocities of air velocity (Ua = 14 m/s) and water velocity (Uw = 0.2 m/s). Simulation A (Ua = 0.11 m/s) had a relatively high liquid holdup value of 0.7987. Simulation B (Ua = 14 m/s) had a significantly lower liquid holdup value of 0.0195. Simulations C, D, E, F, G, and I had the same Ua as in Simulation A and showed similar liquid holdup values as A. Meanwhile, Simulation H & J had the same Ua as in Simulation B and showed similar liquid holdup values as B. Hence, the higher the air velocity, the lower the liquid holdup value.

Simulations A, C, D, E, F, G, and I had the same Uw (Uw = 1.3 m/s) and exhibited relatively high liquid holdup values ranging from 0.6513 to 0.8737. Simulations B, H, and J had the same Uw (Uw = 0.2 m/s) and showed lower liquid holdup values ranging from 0.0097 to 0.0787. Hence, the higher the water velocity, the higher the liquid holdup value. From these comparisons, it could be observed that variations in air velocity (Ua) and water velocity (Uw) had a notable influence on the liquid holdup values.

The next step done was simulation of void fraction following the same steps in liquid hold-up and the results were shown in Figure 21.

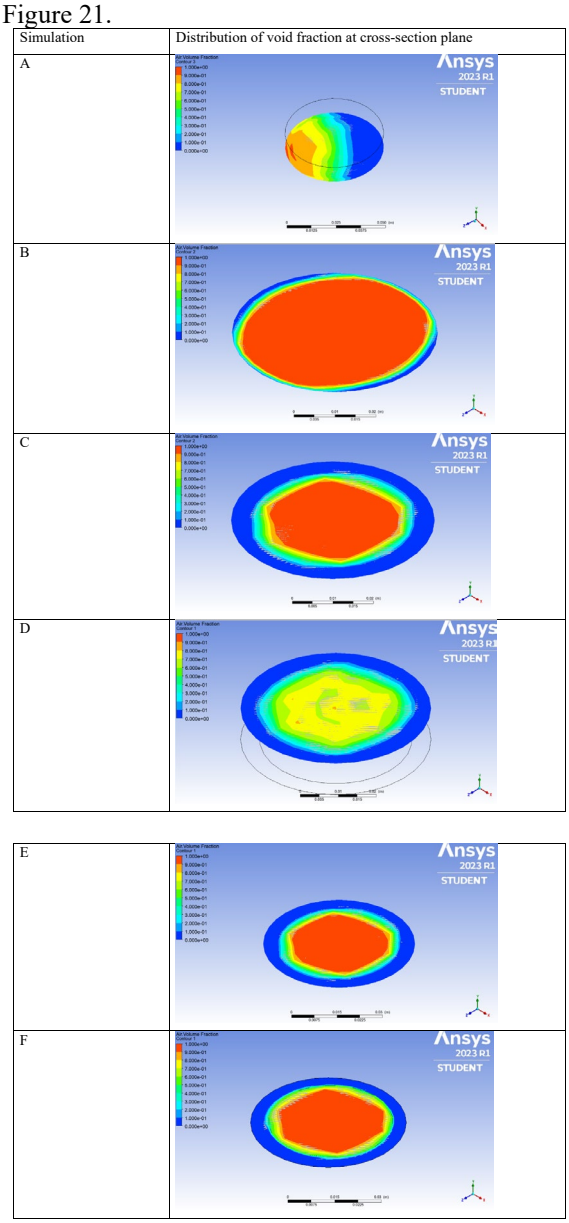

Figure 21: Void Fractions of Simulations

By comparing to simulation A and Simulation B, where the only difference was the velocity of air and water while all other parameters were held constant, the void fraction in Simulation B with higher air velocity and lower water velocity would be expected to be higher than the void fraction in Simulation A with lower air velocity and higher water velocity. Hence, on in a two-phase flow system increased with increasing gas velocity and decreasing liquid velocity.
By comparing Simulation C (k-epsilon RNG) and Simulation D (k-epsilon Realizable), where the only difference was the type of turbulence method while all other parameters were held constant, the air volume fraction in Simulation C was higher than Simulation D. In general, the k-epsilon RNG model is known to provide more accurate results in complex, highly turbulent flows with large separation zones and recirculation regions, while the k-epsilon Realizable model was better suited for flows with moderate turbulence intensity

and moderate Reynolds numbers. Meanwhile, the k-epsilon RNG model was better suited to capture the complex, highly turbulent flow in this case, resulting in higher air volume fraction values for flows with moderate turbulence intensity

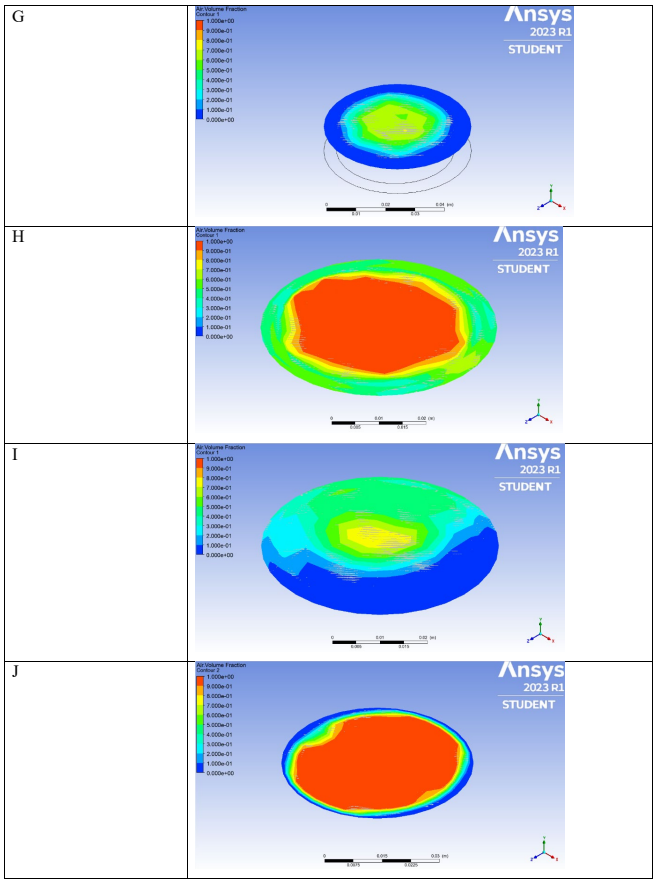

Reynolds numbers. Meanwhile, the k-epsilon RNG model was better suited to capture the complex, highly turbulent flow in this case, resulting in higher air volume fraction values. By comparing Simulation E (k-omega SST) and Simulation F (k-omega standard), where other parameters kept constant while the difference was k-omega turbulence scheme, the result of void fraction was similar. Hence, it appeared that the choice of k-omega turbulence scheme did not significantly impact the predicted void fraction based on the results of Simulation E and Simulation F. By comparing Simulation D (PISO) and Simulation G (SIMPLE), where other parameters kept constant while the difference was Pressure-Velocity Coupling Scheme, the result of void fraction of PISO was clearer than SIMPLE. This was because PISO algorithm was a more advanced and computationally intensive pressure-velocity coupling scheme compared to SIMPLE. PISO algorithm was capable of handling strong density and velocity gradients in the flow more accurately, which might result in a more accurate prediction of void fraction compared to SIMPLE.

The next simulation was liquid film thickness simulation following the same procedures as void fractions. The liquid film thickness in each simulation was influenced by the air velocity, water velocity, turbulence model, and other simulation parameters. Simulation A: With air velocity (Ua) of 0.11 m/s and water velocity (Uw) of 1.3 m/s, the turbulence model used was k-epsilon (Standard). The liquid film thickness was 14 mm. This combination of velocities and turbulence model contributed to a relatively thick liquid film. Simulation B: In this case, Ua was 14 m/s, and Uw was 0.2 m/s. The turbulence model remained k-epsilon (Standard). The resulting liquid film thickness was 2 mm, which was significantly thinner than in Simulation A. The higher air velocity and lower water velocity led to a reduced liquid film thickness.

Table 9: Liquid Film Thickness

Simulation	Liquid film thickness (mm)
A	14
B	2
C	10.8
D	9.5
E	10.65
F	9.6
G	14.4
H	0.01
I	13.8
J	3.5

Simulation C: With Ua at 0.11 m/s and Uw at 1.3 m/s, the turbulence model used was k-epsilon (RNG). The liquid film thickness was 10.8 mm. The change in the turbulence model affected the flow characteristics, resulting in a slightly different liquid film thickness compared to Simulation A. Simulation D: This simulation maintained Ua at 0.11 m/s and Uw at 1.3 m/s but utilized the k-epsilon (Realizable) turbulence model. The liquid film thickness was 9.5 mm. The different turbulence model choice influenced the flow behavior, resulting in a distinct liquid film thickness. Simulations E and F: Both simulations had Ua and Uw values of 0.11 m/s and 1.3 m/s, respectively. The turbulence models used were k-omega (SST) for Simulation E and k-omega (Standard) for Simulation F. The corresponding liquid film thicknesses were 10.65 mm and 9.6 mm, respectively. The choice of turbulence model affected the flow turbulence and consequently the liquid film thickness.

Simulations G and H: These simulations also had Ua and Uw values of 0.11 m/s and 1.3 m/s, respectively. Simulation G utilized the k-epsilon (Realizable) turbulence model with the SIMPLE pressure-velocity coupling scheme, while Simulation H employs the k-epsilon (RNG) turbulence model with the SIMPLE scheme. The resulting liquid film thicknesses were 14.4 mm and 0.01 mm, respectively. The combination of turbulence model and pressure-velocity coupling scheme influences the flow characteristics and led to different liquid film thicknesses. Simulations I and J: These simulations explored the effects of changing the number of time steps and time step size while keeping the velocities and turbulence models the same as in Simulation A and B, respectively. The liquid film thicknesses were 13.8 mm and 3.5 mm for Simulations I and J, respectively. The variations in time step parameters could indirectly influence the flow behavior and subsequently affected the liquid film thickness. Hence, the liquid film thickness in each simulation was influenced by the air velocity, water velocity, turbulence model, pressure-velocity coupling scheme, and other simulation parameters. These factors interacted to determine

the flow pattern and the resulting characteristics of the liquid film in the annular flow regime.

The setup from simulation I was used with the only variation being the air velocity, while keeping all other parameters unchanged. This was important to ensure clearer comparison of the effects of air velocity on flow pattern and pressure drop in simulation. This approach allows for isolating the effect of air velocity on the flow behavior and pressure drop, enabling a more focused analysis. By maintaining consistency in the turbulence model, turbulence scheme, pressure-velocity coupling scheme, number of time steps, and time step size, any observed differences can be attributed primarily to the variation in air velocity. This controlled comparison helped in understanding the specific impact of air velocity on the flow pattern and pressure drop. The simulation results obtained for each case with varying air velocities could be analyzed and compared. Flow patterns could be visualized and classified based on the distribution and behavior of the air and water phases in the vertical pipe. The pressure drop across the pipe could be quantified and compared to assess the influence of air velocity on the resistance to flow Table 10.

Table 10: Air Velocity vs. Pressure Drop

Air Velocity	Flow Pattern	Pressure Drop (Pa)
0.11m/s	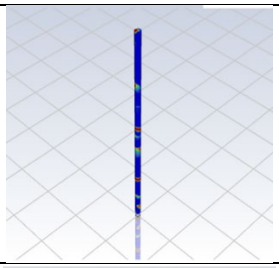	15
0.22m/s	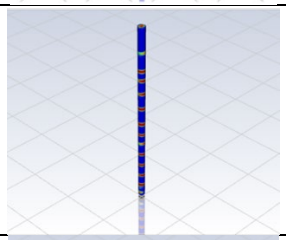	19.2
0.33m/s	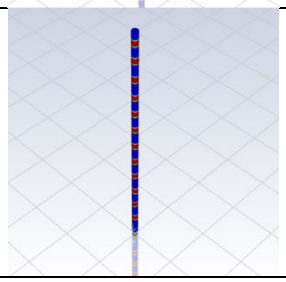	23.7

Based on the data collection, which showed the air velocity and the corresponding pressure drop values in the simulation, a clear trend. As the air velocity increased from 0.11 m/s to 0.22 m/s and then to 0.33 m/s, the pressure drops across the vertical pipe also increased. The pressure drop in a vertical pipe was primarily influenced by the frictional resistance between the flowing fluid (air-water mixture) and the pipe walls. As the air velocity increased, it resulted in higher shear stresses at the pipe walls, leading to increased frictional forces and subsequently a higher pressure drops. When the air velocity was low (0.11 m/s), the flow might be more dispersed, and the air-water mixture experiences relatively lower frictional forces, resulting in a comparatively lower pressure drop of 15pa. However, as the air velocity increased to 0.22 m/s and 0.33 m/s, the flow became more intense and concentrated, leading to increased interaction between the air and water phases and higher frictional forces. This led to a gradual increase in the pressure drop to 19.2pa and 23.7pa, respectively.

The liquid holdup, which indicated the fraction of the pipe's cross-sectional area occupied by the liquid phase (water), decreased with increasing air velocity. The higher velocities promote the disintegration and fragmentation of the liquid film, leading to a reduced liquid holdup in the pipe. The void fraction, which represented the fraction of the pipe's cross-sectional area occupied by the gas phase (air), increased. This was attributed to the higher air velocities causing increased entrainment and dispersion of the air within the water phase, resulting in a larger volume fraction of gas in the pipe. Liquid film thickness, the increase in air velocity also led to a decrease in the liquid film thickness, which refered to the depth of the liquid phase adhering to the pipe walls. The intensified shearing and turbulence caused by higher air velocities result in a thinner liquid film along the pipe walls.

CONCLUSION

The optimum number of mesh elements for mesh independence study was proposed. After evaluating different mesh configurations, it was determined that the multizone mesh with 5 layers of inflation, consisting of 114,600 nodes and 107,587 elements, yielded the most accurate and reliable results. This mesh configuration is recommended for future simulations in similar applications. The effect of flow regime based on the selection of turbulence scheme was evaluated.

This reaffirmed the importance of turbulence model selection in predicting and understanding the behavior of gas-liquid flows in vertical pipes. Specifically, when the water velocity was 1.3 m/s and the air velocity was 0.11 m/s, the flow regime was identified as slug flow. To accurately capture the turbulent flow with bubble and slug flow patterns, the K-ε (Realizable) turbulence model was utilized as mentioned in the previous research. This turbulence model was known for its ability to handle complex flows with large-scale turbulence structures and was suitable for capturing the characteristics of slug flow. On the other hand, when the water velocity was 0.2 m/s and the air velocity was 14 m/s, the flow regime was identified as annular flow. To accurately simulate annular flow, the RNG turbulence model was used same as the previous research. The RNG model is known for its ability to capture the flow characteristics in annular flow and churn flow patterns, where the flow was more dispersed and has a higher gas-liquid interface.

Lastly, the influence of hold-up, void fraction, and liquid film thickness on pressure drop through the vertical pipes was compared. The findings revealed a clear relationship between these parameters and pressure drop. As the pressure drop increased, the liquid hold-up decreased, the void fraction increased, and the liquid film thickness decreased. The decrease in liquid hold-up with increasing pressure drop can

be attributed to the increased momentum of the flow. As the pressure drop rises, the flow velocity increases, leading to a more efficient entrainment of the liquid phase. This resulted in a lower liquid hold-up in the pipe.

The increase in void fraction with pressure drop could be explained by the increased gas velocity and turbulence in the system. As the pressure drop rose, the gas phase experienced higher velocities, which promoted better dispersion and breakup of the liquid phase. This led to a higher void fraction, indicating a greater volume occupied by gas relative to the total volume. The decrease in liquid film thickness with increasing pressure drop is a consequence of the intensified shear forces between the gas and liquid phases. As the pressure drop rose, the flow became more vigorous, leading to enhanced interaction and mixing between the gas and liquid. This resulted in a thinner liquid film adhering to the pipe walls.

Overall, this research project significantly contributed to the understanding and optimization of gas-liquid flow in vertical pipelines. The proposed optimum mesh configuration validated turbulence scheme selection, and insights into the influence of flow parameters on pressure drop, hold-up, void fraction, and liquid film thickness provided valuable guidance for future studies and engineering applications in this field.

ACKNOWLEDGMENT

We would like to thank Asia Pacific University for giving us the opportunity to conduct this paper.

REFERENCES

1. Abdulkadir, M., Hernandez-Perez, V., Lo, S., Lowndes, I., & Azzopardi, B. (2015). Comparison of experimental and Computational Fluid Dynamics (CFD) studies of slug flow in a vertical riser. *Experimental Thermal and Fluid Science*, 468-483.
2. Adaze, E., Badr, H. M., & Al-Sarkhi, A. (2019). CFD modeling of two-phase annular flow toward the onset of liquid film reversal in a vertical pipe. *Journal of Petroleum Science and Engineering*, 755-774.
3. Chen, L., Tian, Y., & Karayiannis, T. (2006). The effect of tube diameter on vertical two-phase flow regimes in small tubes. *Int J Heat Mass Transf*, 4220-4230.
4. Cheng, H., Hills, J., & Azzorpardi, B. (1998). A study of the bubble-to-slug transition in vertical gas-liquid flow in columns of different diameter. *Int J Multiph Flow.*, 431-451.
5. Ganat, T., & Hrairi, M. (2018). Gas–Liquid Two-Phase Upward Flow through a Vertical Pipe: Influence of Pressure Drop on the Measurement of Fluid Flow Rate. . *Energies*.
6. Gardenghi, Á., Filho, E. D., Chagas, D. D., Scagnolatto, G., Oliveira, R. J., & Tibiriçá, C. B. (2020). Overview of Void Fraction Measurement Techniques, Databases and Correlations for Two-Phase Flow in Small Diameter Channels . *Fluids*, 216.
7. Gayet, C., Diaye, M., & Line, A. (2013). Behaviour of slug flow and pressure force induced in a spool: numerical simulation of a Taylor bubble flowing in a liquid flow through a spool. *16th International Conference on Multiphase Production Technology.* BHR Group.
8. Gray, G. S., & Ormiston, S. J. (2021). A comparative study of closure relations for CFD modelling of bubbly flow in a vertical pipe . *Open Journal of Fluid Dynamics*, 98-134.
9. Hibiki, T., & Mishima, K. (2001). Flow regime transition criteria for upward two-phase flow in vertical narrow rectangular channels. *Nucl Eng Des.* , 117-131.
10. Kiran, R., Ahmed, R., & Salehi, S. (2020). Experiments and CFD modelling for two phase flow in a vertical annulus 2020. *Chemical Engineering Research and Design*, 201-211.
11. Li, P., Zhang, X., & Lu, X. (2019). Three-dimensional Eulerian modeling of gas–liquid–solid flow with gas hydrate dissociation in a vertical pipe. *Chemical Engineering Science*, 145-165.
12. Li, Z., Wang, G., Yousaf, M., Yang, X., & Ishii, M. (2018). Flow structure and flow regime transitions of downward two-phase flow in large diameter pipes. *International Journal of Heat and Mass Transfer*, 812-822.
13. Liang, Z., Guo, C., & Wang, C. (2021). The connection between flow pattern evolution and vibration in 90-degree pipeline: Bidirectional fluid-structure interaction., . *Energy Science & Engineering*, 308-323.
14. Liu, C. L., Sun, Z., Lu, G. M., Song, X. F., & Yu, J. G. (2015). Experimental and numerical investigation of two-phase flow patterns in magnesium electrolysis cell with non-uniform current density distribution. . *The Canadian Journal of Chemical Engineering*, 565-579.
15. Lote, D. A., Vinod, V., & Patwardhan, A. W. (2018). Computational Fluid Dynamics Simulations of the Air-Water Two-Phase Vertically Upward Bubbly Flow in Pipes. *Industrial & Engineering Chemistry Research*, 10609-10627.
16. Mahmood, R. A. (2019). CFD Instruction Guide to Simulate Two-Phase Flow Separation in a Vertical T-junction Separator. *International Journal of Advances in Science Engineering and Technology*.
17. Mishima, K., & Ishii, I. (1984). Flow regime transition criteria for two-phase flow in vertical tubes. *Int. J. Heat Mass Transfer*, 723-734.
18. Razzaghi, A., Amjad, A., & Maleki, M. (2020). Thickness measurement of transparent liquid films with Paraxial Self-Reference Interferometry. *Scientific Reports*.
19. Ren, G., Ge, D., Li, P., Chen, X., Zhang, X., Lu, X., . . . Su, F. (2021). The Flow Pattern Transition and Water Holdup of Gas–Liquid Flow in the Horizontal and Vertical Sections of a Continuous Transportation Pipe. *Water*, 2077.
20. Shawkat, M., Ching, C., & Shoukri, M. (2008). Bubble and Liquid Turbulence Characteristics of Bubbly Flow in a Large Diameter Vertical Pipe. *International Journal of Multiphase Flow*, 767-785.
21. Sim, W., Bae, B., & Mureithi, N. (2010). An experimental study on characteristics of two-phase flows in vertical pipe. *J Mech Sci Technol*, 1981-1988.
22. Wang, M., Zheng, D., & Xu, Y. (2019). A new method for liquid film thickness measurement based on ultrasonic

echo resonance technique in gas-liquid flow. *Measurement*, 447-457.

23. Wongwises, S., & Pipathattakul, M. (2006). Flow pattern, pressure drop and void fraction of two-phase gas–liquid flow in an inclined narrow annular channel. *Experimental Thermal in journal of Fluid Science*, 345-354.
24. Xu, Q., Wang, X., Chang, L., Wang, J., Li, Y., Li, W., & Guo, L. (2022). Signal optimization for recognition of gas–liquid two-phase flow regimes in a long pipeline-riser system. *Measurement*, 200.
25. Yadav, M. S., Kim, S., Tien, K., & S. M. Bajorek. (2014). Experiments on geometric effects of 90-degree vertical-upward elbow in air water two-phase flow. *" International Journal of Multiphase Flow*, 98-107.
26. Yang, H. (2020). The effect of interfacial mass transfer of slip-rising gas bubbles on two-phase flow in the vertical wellbore/pipeline. *International Journal of Heat and Mass Transfer*, 119326.